

Single-Molecule Device Prototypes for Protein-Based Nanoelectronics: Negative Differential Resistance and Current Rectification in Oligopeptides

David M. Cardamone and George Kirczenow

Physics Department, Simon Fraser University, Burnaby, BC V5A 1S6, Canada

We investigate electrical conduction through individual oligopeptide molecules thiol-bonded between gold nanocontacts using *ab initio* and semi-empirical techniques. Our theory explains for the first time these molecules' experimentally observed current-voltage characteristics, including both the magnitude and rectification of the current. We identify the mechanism of the observed current rectification, and predict that it will result in negative differential resistance at moderate biases. Our findings open the way to the realization of protein-based nanoelectronic devices.

PACS numbers: 81.07.Nb, 73.63.-b, 85.65.+h, 87.14.Ee

I. INTRODUCTION

Living cells survive and function through their unique ability to manufacture a vast catalog of specific molecules repeatably and reliably, a capacity long recognized to hold promise for the design of nanoelectronic devices.¹ Whereas much experimental and theoretical work has been devoted to understanding the electron transport properties of single nucleic acid molecules, relatively little has focused on the same qualities of other biomolecules. In particular, over the course of its life a cell produces far more polypeptide chains than DNA sequences, while amino acids, the building blocks of proteins, display five times more diversity than DNA bases. As such, the single-molecule electron transport characteristics of these protein fragments, and of entire proteins, is a field with great potential, which is only beginning to be explored.

Recently, experimentalists have succeeded in addressing the effects of primary protein structure, *i.e.* specific amino acid sequences, on conductance.^{2,3} These experiments, applying the STM-break junction (STMBJ) technique^{4,5,6} to oligopeptide molecules, present an exciting new approach to biologically-based nanoelectronic devices: They offer a broad class of well defined experimental systems operating at length scales on which coherent quantum effects are dominant. Reference 3, in particular, demonstrated this promise with non-equilibrium results evincing a striking current rectification.

The purpose of this article is to present the first theoretical treatment of electron transport through these systems. We explain the phenomena observed in these experiments, in particular the current rectification, by use of Landauer conductance theory,⁷ and demonstrate good quantitative agreement with the experimental data. We show that the rectification is the result of resonance between gold-molecule interfacial states partially localized on either side of the molecule (see Fig. 1); these states are detuned from each other in equilibrium due to the oligopeptides' intrinsic asymmetry. Moreover, we predict that, at moderately higher voltages, a related mechanism will generate negative differential resistance (NDR), *i.e.*, a decrease in current with increased bias voltage; this phenomenon has important device applications, includ-

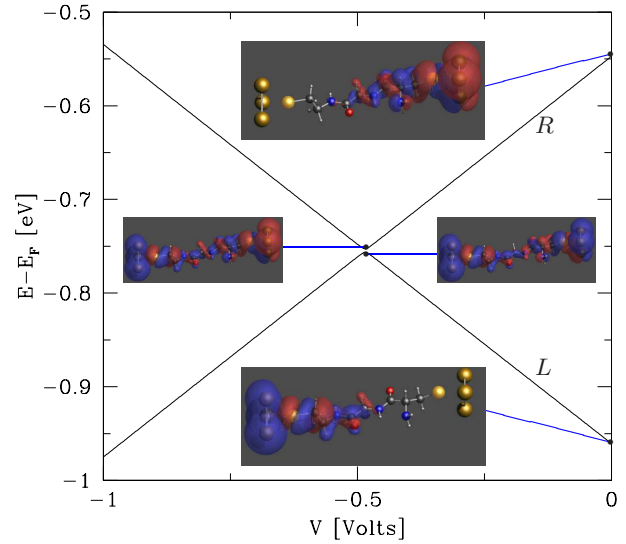


FIG. 1: (Color online) Anticrossing of generalized eigenstates R and L of the simplified extended molecule discussed in the text for cysteamine-Gly-Cys bonded to two hollow sites in the Au(111) leads. In the full system, the anticrossing's abruptness is tempered by broadening from the leads. The insets show the states at specific bias voltages.

ing low-noise amplification,⁸ high frequency oscillators,⁹ analog-to-digital conversion,¹⁰ and digital logic.¹¹ Thus, our findings open the way to the realization of practical oligopeptide, and ultimately protein-based, nanoelectronic devices.

We organize the paper as follows. Section II presents the theoretical formalism we use to model charge transport through metal-oligopeptide-metal junctions. In Section III, we discuss our results for these systems, including determination of the experimental geometry, explanation of their rectifying properties, and prediction of NDR. Section IV summarizes our main conclusions.

II. MODEL

To determine the molecular geometry in the presence of the gold leads, we apply a series of density functional theory *ab initio* calculations to relax the molecule between two fixed gold atoms.¹² At each step, the distance between the two atoms is increased slightly, and the geometry relaxed again, to simulate the stretching the molecule undergoes in an STMBJ experiment. For calculations reported here, the molecules have been stretched to their greatest length before breakage occurs, although we find that less stretched molecules have essentially the same conductance features and order of magnitude. In the case of hollow binding sites, we replace the gold atom with the three nearest-neighbor gold atoms, and relax the molecule one final time.

To determine conductance and current, we first partition the metal-oligopeptide-metal system into left and right macroscopic gold electrodes, and an extended molecule containing the central organic molecule as well as 50-100 atoms of each Au(111) contact. The Hamiltonian of the full system is therefore the sum of two terms:

$$H = H_{mol} + H_{leads}. \quad (1)$$

H_{mol} describes the isolated extended molecule, and H_{leads} does the same for the macroscopic electrodes, as well as containing the quantum mechanical coupling between them and the extended molecule.

We employ a semi-empirical model for H_{mol} ; such models are known to be highly effective in predicting, reproducing, and explaining experimental results for metal-organic molecule-metal junctions (*e.g.*, Ref. 13, Ref. 14 and the results of Refs. 15 and 6, Ref. 16). The Hamiltonian of the full extended molecule is given by extended Hückel theory.^{17,18,19,20,21,22}

H_{leads} provides both decoherent broadening and elastic scattering to the discrete states of the extended molecule. To model this, we assign semi-infinite, one-dimensional leads²³ to each gold orbital not immediately adjacent to the oligopeptide; their number is equal to the coordination number of gold minus the number of nearest-neighbor atoms included in the extended molecule. We take the intersite hopping within each lead, as well as the hopping between lead and orbital, to be 5eV. These choices quantitatively reproduce the quantized conductance^{24,25} of a gold quantum point contact.

The open system described by H requires an infinite Fock space. To solve the full molecule-plus-leads system, then, we make use of Dyson's Equation, which gives the retarded Green function

$$G(E) = [G_{mol}^{-1}(E) - \Sigma(E)]^{-1}. \quad (2)$$

Here

$$G_{mol}(E) = \frac{1}{SE - H_{mol} + i0^+} \quad (3)$$

is the Green function for the extended molecule only,²⁶ and the retarded self-energy $\Sigma(E)$ is given by Ref. 23.

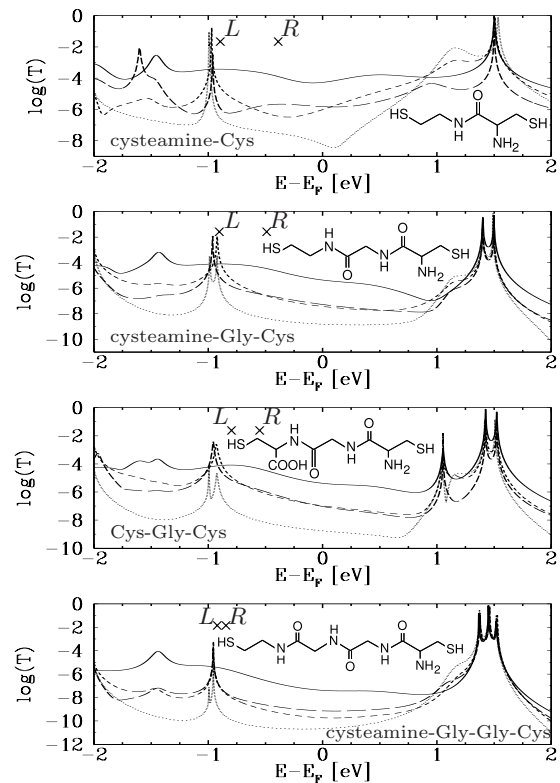


FIG. 2: Equilibrium transmission functions $T(E, 0)$ for various bonding geometries for each of the four oligopeptide molecules studied experimentally in Refs. 2 and 3. Solid lines indicate hollow-site bonding geometry on both sides. Dotted: top-site at both metal-molecule interfaces. Long dashes: hollow-site bonding for the sulfur on the amine-terminated side of the molecule and top-site bonding for the other. Short dashes: *vice versa*. Experimental conductances agree well with the solid curves in all cases. For the hollow-hollow geometry, the energies of the two molecular orbitals responsible for rectification are indicated with crosses. Inset: Structural formulae of the gas-phase molecules. When bonded to gold, the terminating hydrogen atoms are lost.

S is the atomic orbital overlap matrix of the extended molecule. Equation (2) thus represents an exact method to incorporate the effects of H_{leads} into transport.

We model electrostatic effects, including the potential imposed by the contacts as well as screening by the free ionic charges in the electrolyte solution surrounding the molecule, with a linearized Debye-Hückel theory.²⁷ Poisson's equation for the total electric potential $\Phi(\mathbf{r})$ becomes

$$\nabla^2 \Phi(\mathbf{r}) = \frac{2n}{k_B T \epsilon} \Phi(\mathbf{r}), \quad (4)$$

where $n = .1\text{M}$ is the concentration of the solution, ϵ is the dielectric constant of water, and $k_B T$ is room temperature. After solving Eq. (4) for parallel-plate boundary conditions, the potential is applied to H_{mol} :²⁸

$$(H_{mol})_{ij} \rightarrow (H_{mol})_{ij} - eS_{ij} \frac{\Phi(\mathbf{r}_i) + \Phi(\mathbf{r}_j)}{2} \quad (5)$$

TABLE I: Comparison of the conductances found in our model (in units of g_0) for various bonding geometries with those of the STMBJ experiments.^{2,3} In the column headings, the first entry indicates the bonding geometry on the amine side of the molecule, the second the other. Only hollow bonding at both interfaces is compatible with experiment.

molecule	experimental	hollow-hollow	hollow-top	top-hollow	top-top
cysteamine-Cys	1.8×10^{-4}	5.4×10^{-5}	1.5×10^{-6}	9.6×10^{-7}	5.8×10^{-9}
cysteamine-Gly-Cys	4.2×10^{-6}	4.3×10^{-6}	5.3×10^{-8}	3.7×10^{-8}	1.5×10^{-9}
Cys-Gly-Cys	5.3×10^{-6}	4.2×10^{-6}	9.3×10^{-8}	1.0×10^{-7}	1.7×10^{-9}
cysteamine-Gly-Gly-Cys	5.0×10^{-7}	4.1×10^{-8}	7.3×10^{-10}	1.9×10^{-10}	2.2×10^{-11}

Here, \mathbf{r}_i is the position of the i^{th} atomic orbital. The site energies of each lead shift uniformly with its metallic contact's electrostatic potential. All the quantities in Eq. (2) thus become functions of the applied bias V .

The Landauer formalism⁷ yields the conductance and current through the molecule. The probability for an electron of energy E to move from the left set of leads to the right is

$$T(E, V) = \sum_{\substack{\alpha \in \text{left} \\ \beta \in \text{right}}} \text{Tr} \left[\Gamma^{(\beta)}(E, V) G(E, V) \Gamma^{(\alpha)}(E, V) G^\dagger(E, V) \right], \quad (6)$$

where

$$\Gamma^{(\alpha)}(E, V) \equiv -2 \text{Im} \left[\Sigma^{(\alpha)}(E, V) \right] \quad (7)$$

is the broadening function for the term of Σ from lead α . The zero-bias conductance of the metal-molecule-metal junction is $g = g_0 T(E_F, 0)$, with the conductance quantum $g_0 = 2e^2/h$ and the bulk gold Fermi energy E_F evaluated for a 500-atom spherical gold nanocluster. The current is⁷

$$I(V) = \frac{e}{h} \int_{-\infty}^{\infty} dE T(E, V) [f(E - \mu_L) - f(E - \mu_R)], \quad (8)$$

where $f(E - \mu_{L,R})$ is the Fermi function of the leads on the left (right) side of the extended molecule, and $\mu_{L,R}(V)$ is the corresponding electrochemical potential.

III. RESULTS AND DISCUSSION

A. Conductance and Bonding Geometry

We studied the conductance and current of each oligopeptide molecule measured experimentally in Refs. 2 and 3, varying several parameters of the experimental geometry in each case. These included the sulfur-to-sulfur distance as the molecule was stretched, the presence of additional molecules of the self-assembled monolayers, and bond geometry; only the last was found to have a significant impact on the observables. Figure 2 demonstrates this dependence, considering all four possibilities involving the two most likely bonding geometries of the sulfur:²⁹ either directly to a single gold atom on top of the

Au(111) substrate, or above a triangular hollow. Table I compares the conductances obtained from our model with experiment.

The experimental data are consistent only with the model calculations for a hollow bonding geometry on both ends of each oligopeptide molecule. Since this model is known to produce quantitatively correct conductance in other gold-thiol systems,^{13,14,16} we conclude that this is indeed the experimental geometry, and that the orders-of-magnitude smaller conductances associated with more weakly bound molecules, or with molecules bound via monatomic gold chains, form part of the low-conductance noise in the experimental histograms.² In this way, the statistical histograms of the STMBJ technique yield a specific geometry for the metal-molecule-metal junction, despite sulfur's ability to bond to a gold substrate in several geometries.

To understand the transmission curves, it is helpful to think in terms of a smaller extended molecule which includes only the two to six gold atoms to which the sulfurs bond. Transmission states near E_F correspond to gold-sulfur interfacial orbitals of this simplified extended molecule. Because there are two metal-molecule interfaces, these states typically occur in pairs with similar energies. When the two states are detuned from each other, they are largely localized at either end of the molecule; when in resonance, they mix into bonding and antibonding combinations (see Fig. 1). For a symmetric extended molecule at zero bias, the pairs are always in resonance; oligopeptides, however, are intrinsically asymmetric, so interfacial states can be detuned from each other and localized at either end, even in equilibrium.

Prominent peaks in the transmission spectra (Fig. 2) occur near the energies of molecular orbitals which bridge the left and right leads. Thus, the resonances, and consequent hybridization, of levels otherwise localized on opposite ends of the extended molecule play a dominant role in determining electron transport. For example, in all molecules and bonding configurations studied here, the two levels immediately below E_F are paired interfacial states, which we call R (localized at the gold-molecule interface near the amine terminus of the molecule) and L (localized at the other interface). The narrow transmission peaks associated with their bonding and antibonding combinations are visible 1eV below E_F in the double on-top (dotted) curves of Fig. 2. Because the overlap of the gold $6s$ and sulfur $3p$ orbital is strongly

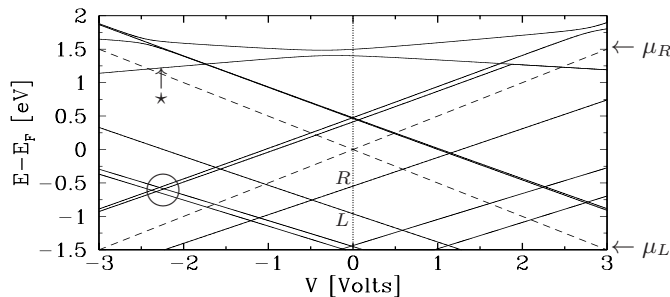


FIG. 3: Movement with applied bias of the generalized eigenvalues of the six-gold-atom simplified extended molecule for cysteamine-Gly-Cys in the hollow-hollow configuration. Some lines are doubled by degrees of freedom in the gold contacts; when more gold atoms are included, the molecular orbitals split further, eventually developing into the continuous density of states of an infinite system. Note that the apparent intersections are actually avoided crossings. In equilibrium, states R and L are detuned by $.4\text{eV}$ due to molecular asymmetry. They come into resonance only under negative bias, causing current rectification. Without these two states, the location of anticrossings, and thus the I - V characteristic, would be largely symmetric. The dashed lines represent the electrochemical potentials of the right and left electrodes, μ_R and μ_L . NDR is the results of increasing bias beyond the last anticrossing in a group; an example is circled.

angle dependant,³⁰ these peaks each become broadened when their respective bonding geometries are changed to hollow. Furthermore, the hollow-bonded versions of R are more sensitive to the asymmetric features of the oligopeptide molecules, resulting in a significant detuning from L (shown by the crosses in Fig. 2). The transmission peak associated with these two states is thus also severely broadened, becoming a smooth shoulder in $T(E, 0)$.

B. Current Rectification

The movement and change under bias of R and L , depicted in Fig. 1, give rise to the rectification observed by Xiao *et al.* in Ref. 3. Positive bias raises (lowers) the electrochemical potential of atomic orbitals on the amine (non-amine) side of the molecule; consequently, under negative bias the energies of R and L move closer together. Near resonance, R and L hybridize into whole-molecule states, allowing significant charge transport.

Figure 3 shows the movement under bias of several generalized eigenenergies of the simplified extended molecule for hollow-hollow bonded cysteamine-Gly-Cys. All of the states in the region around E_F occur in right/left pairs like R and L , but only R and L are detuned from each other in equilibrium. Without R and L , the locations of anticrossings are nearly symmetric about $V = 0$. Rectification is a result of the splitting between these two states, itself a direct consequence of oligopeptide asymmetry.

Figure 4 gives the calculated current-voltage character-

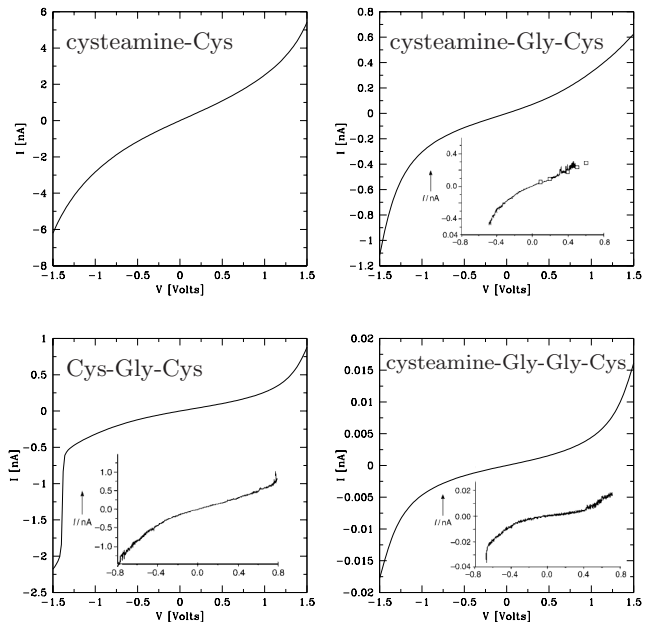


FIG. 4: Calculated current-voltage characteristics of four single-molecule oligopeptide devices. The scale and asymmetry of the current are comparable to those found in the experimental studies of Ref. 3, reproduced here in inset.

istic for each molecule, showing this rectification. While the resonance depicted in Fig. 1 is comparatively narrow and outside the energy window between μ_L and μ_R , rectification extends beyond 2V in the full systems due to the strong hollow-site broadening of R and L . For the three molecules for which Xiao *et al.* made I - V measurements (shown in inset), the calculated rectification is in excellent qualitative agreement with experimental data. We find a current ratio of about 150% for cysteamine-Gly-Cys and Cys-Gly-Cys, similar to Ref. 3. Cysteamine-Gly-Gly-Cys exhibits less rectification, both in our model and the experimental data: This is due to its much smaller detuning between R and L at zero bias.

C. Negative Differential Resistance

Negative differential resistance ($dI/dV < 0$) can result from applied bias destroying a resonance between transmitting interfacial states.^{31,32} As the bias increases past an anticrossing in the metal-oligopeptide-metal systems, the two interfacial states are taken further apart in energy. They therefore mix less well, and become localized at the individual metal-molecule interfaces. As the bias voltage increases, then, electron transport through these states “shuts off”, creating the potential for NDR.

Such effects are masked while the current is still small: The dominant effect is the increasing current from a series of crossings and states entering the window of integration. Nevertheless, once the voltage is large enough

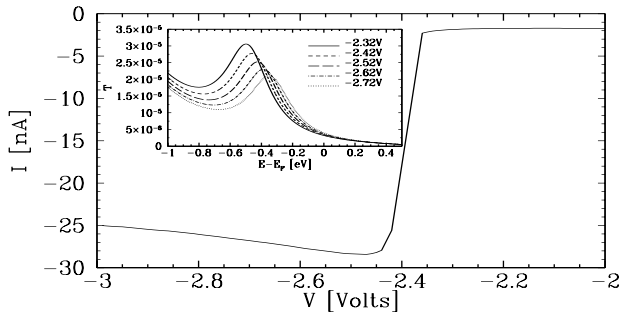


FIG. 5: I - V characteristic for the hollow-hollow gold-cysteamine-Gly-Cys-gold system in the medium-bias regime, showing NDR. Other oligopeptide molecules have qualitatively similar characteristics. (inset) Corresponding $T(E, V)$ curves. NDR corresponds to a gradual decrease in the transmission peak's strength as voltage becomes more negative, due to departure from a resonant crossing of interfacial states (the circle in Fig. 3).

that an entire neighborhood of interfacial resonances has been encompassed, further applied bias yields NDR. One such crossing is indicated by the circle in Fig. 3; its I - V characteristic and relevant transmission properties are shown in Fig. 5. As V becomes more negative, the peak in $T(E)$ associated with the nearly degenerate hybridized states diminishes. After the final current step, due to a mid-molecule orbital (\star in Fig. 3) entering the window of integration, NDR results. The bias voltages required to observe this important phenomenon are only moderately larger than those already achieved experimentally.³

IV. CONCLUSIONS

Like their rectifying properties, the NDR that we predict in oligopeptides is a direct result of the dominance of resonant crossings of interfacial states in charge transport. Since this is a property of all thiol- (*i.e.* cysteamine- or cysteine-) bonded oligopeptide molecules, both effects are robust, and observable in the entire class of such molecules. Because of the limitless customizability and simple fabrication of oligopeptides, the effects can be tailored to meet a wide variety of device needs.

In summary, we have developed a theoretical model which explains all of the experimental data on charge transport through oligopeptide molecules. The model generates quantitatively accurate conductances, and reproduces the striking diode-like behavior found in experiment. Furthermore, it predicts NDR, a phenomenon of vital importance for many device applications. Oligopeptides offer a unique combination of customizability and scalability, and it is our hope that this work will inspire much further study of their electron transport properties.

Acknowledgments

We thank Nongjian Tao, Joshua Hihath, and Ross Hill for useful discussions. This work was supported by NSERC and the Canadian Institute for Advanced Research.

-
- ¹ R. I. Gilmanishin, In K. Siemicki, ed. *Molecular Electronics and Molecular Electronic Devices, Vol. 2* (CRC Press, Boca Raton, 1993), pp. 1–78.
 - ² X. Xiao, B. Xu, and N. Tao, *J. Am. Chem. Soc.* **126**, 5370 (2004).
 - ³ X. Xiao, B. Xu, and N. Tao, *Angew. Chem. Int. Ed.* **43**, 6148 (2004).
 - ⁴ B. Xu and N. J. Tao, *Science* **301**, 1221 (2003).
 - ⁵ B. Xu, X. Xiao, and N. J. Tao, *J. Am. Chem. Soc.* **125**, 16164 (2003).
 - ⁶ X. Xiao, B. Xu, and N. J. Tao, *Nano Lett.* **4**, 267 (2004).
 - ⁷ S. Datta, *Electron Transport in Mesoscopic Systems*, vol. 3 of *Cambridge Studies in Semiconductor Physics and Microelectronic Engineering* (Cambridge University Press, Cambridge, UK, 2003), ISBN 0 521 59943 1.
 - ⁸ A. van der Ziel, *Solid-State Electron.* **26**, 333 (1983).
 - ⁹ E. R. Brown, J. R. Söderström, C. D. Parker, L. J. Mahoney, K. M. Molvar, and T. C. McGill, *Appl. Phys. Lett.* **58**, 2291 (1991).
 - ¹⁰ T. P. E. Broekaert, B. Brar, J. P. A. van der Wagt, A. C. Seabaugh, F. J. Morris, T. S. Moise, E. A. Beam, III, and G. A. Frazier, *IEEE J. Solid-State Circuits* **33**, 1342 (1998).
 - ¹¹ R. H. Mathews, J. P. Sage, T. C. L. G. Sollner, S. D. Calawa, C.-L. Chen, L. J. Mahoney, P. A. Maki, and K. M. Molvar, *Proc. IEEE* **87**, 596 (1999).
 - ¹² Gaussian 98, Revision A.11.3, M. J. Frisch *et al.*
 - ¹³ S. Datta, W. Tian, S. Hong, R. Reifenberger, J. I. Henderson, and C. P. Kubiak, *Phys. Rev. Lett.* **79**, 2530 (1997).
 - ¹⁴ E. G. Emberly and G. Kirczenow, *Phys. Rev. B* **64**, 235412 (2001).
 - ¹⁵ M. A. Reed, C. Zhou, C. J. Muller, T. P. Burgin, and J. M. Tour, *Science* **278**, 252 (1997).
 - ¹⁶ J. G. Kushmerick, D. B. Holt, J. C. Yang, J. Naciri, M. H. Moore, and R. Shashidhar, *Phys. Rev. Lett.* **89**, 086802 (2002).
 - ¹⁷ R. Hoffman, *J. Chem. Phys.* **39**, 1397 (1963).
 - ¹⁸ J. H. Ammeter, H.-B. Bürgi, J. C. Thibault, and R. Hoffman, *J. Am. Chem. Soc.* **100**, 3686 (1978).
 - ¹⁹ J. Cerdá and F. Soria, *Phys. Rev. B* **61**, 7965 (2000).
 - ²⁰ G. Kirczenow, P. G. Piva, and R. A. Wolkow, *Phys. Rev. B* **72**, 245306 (2005).
 - ²¹ D. Kienle, J. I. Cerda, and A. W. Ghosh, *J. Appl. Phys.* **100**, 043714 (2006).
 - ²² The numerical implementation used was the YAeHMOP package (ver. 3.0), by G. A. Landrum and W. V. Glassey.
 - ²³ V. Mujica, M. Kemp, and M. A. Ratner, *J. Chem. Phys.* **101**, 6856 (1994).

- ²⁴ K. Hansen, S. K. Nielsen, M. Brandbyge, E. Lægsgaard, I. Stensgaard, and F. Besenbacher, *Appl. Phys. Lett.* **77**, 708 (2000).
- ²⁵ H. Mehrez, A. Wlasenko, B. Larade, J. Taylor, P. Grütter, and H. Guo, *Phys. Rev. B* **65**, 195419 (2002).
- ²⁶ E. Emberly and G. Kirczenow, *Phys. Rev. Lett.* **81**, 5205 (1998).
- ²⁷ L. D. Landau and E. M. Lifshitz, *Statistical Physics*, vol. 5 of *Course of Theoretical Physics* (Pergamon, Bristol, Great Britain, 1958).
- ²⁸ E. G. Emberly and G. Kirczenow, *Chem. Phys.* **281**, 311 (2002).
- ²⁹ X. Li, J. He, J. Hihath, B. Xu, S. M. Lindsay, and N. Tao, *J. Am. Chem. Soc.* **128**, 2135 (2006).
- ³⁰ The effect of bond geometry on molecular transmission has been well studied. See, for example, E. G. Emberly and G. Kirczenow, *Phys. Rev. B* **58**, 10911 (1998); M. Di Ventura, S. T. Pantelides, and N. D. Lang, *Phys. Rev. Lett.* **84**, 979 (2000); P. E. Kornilovitch and A. M. Bratkovsky, *Phys. Rev. B* **64**, 195413 (2001); C. Toher, A. Filippetti, S. Sanvito, and K. Burke, *Phys. Rev. Lett.* **95**, 146402 (2005).
- ³¹ H. Dagleish and G. Kirczenow, *Nano Lett.* **6**, 1274 (2006).
- ³² H. Dagleish and G. Kirczenow, *Phys. Rev. B* **73**, 245431 (2006).